

<https://doi.org/10.1038/s44303-025-00078-y>

MRI detection of senescent cells in porcine knee joints with a β -galactosidase responsive Gd-chelate



Kerem Nernekli^{1,6}, Dilyana B. Mangarova^{1,6}, Vidyani Suryadevara^{1,6}✉, Mohammadjavad Hajipour¹, Jian-Hong Tang², Jie Wang¹, Tie Liang¹, Marek Harris¹, Tsuyoshi Ueyama³, Jennifer K. Lyons³, Michael E. Moseley¹, Raheleh Roudi¹, Laura Pisani¹, Ricarda von Krüchten¹, Ramesh Duwa¹, Sarah Ying Lu-Liang¹, Zahra Shokri Varniab¹, Iryna Vasyli¹, Neeladrisingha Das⁴, Masatoshi Murayama⁵, Issei Shinohara⁵, Guillem Pratx⁴, Stuart B. Goodman⁵, Thomas J. Meade^{2,7}✉ & Heike E. Daldrup-Link^{1,7}✉

Senescent cells promote osteoarthritis progression through the secretion of inflammatory mediators. Preclinical studies have identified senescence-associated beta-galactosidase (β -gal) as a biomarker of senescence, but in vivo detection remains challenging. Here, we evaluated whether a β -gal responsive gadolinium (Gd) chelate can non-invasively detect β -gal expressing senescent cells with standard clinical magnetic resonance imaging (MRI) technology in vitro, ex vivo, and in vivo in porcine joints. In vitro studies showed that senescent mesenchymal stromal cells (MSCs) exhibited significant MRI signal enhancement upon incubation with the β -gal responsive Gd-chelate compared to viable control cells. In vivo, intraarticular injection of the probe into pig knee joints revealed its retention and activation by senescent cells in cartilage defects, evidenced by a significant increase in R_1 relaxation rate. MRI-based senescent cell detection holds promise for identifying patients amenable to senolytic therapies, tailoring treatment plans, and monitoring therapy response in real-time.

Osteoarthritis (OA), the most common chronic joint disease, is characterized by joint pain, limited motion, and joint stiffness¹. While the typical course of OA involves slow, progressive joint damage over many years, some patients experience rapid progression. Recent evidence implicates senescent cells in cartilage and synovium as key players in OA development, highlighting their potential as therapeutic targets². Senescent cells undergo replicative arrest and develop a senescence-associated secretory phenotype (SASP), characterized by the secretion of chemokines, inflammatory cytokines, and matrix-degrading proteases^{3,4}. These mediators contribute to cartilage degradation and eventual joint destruction, leading to OA⁵. Various senolytic therapies, such as dasatinib⁶, quercetin⁷, navitoclax⁸, and metformin⁹, have entered clinical trials, demonstrating promising results in slowing the progression of OA and improving clinical symptoms¹⁰. However, despite the rapid development of senolytic therapies for OA treatment, no imaging technology is currently capable of detecting senescent cells in vivo or in patients. A clinically translatable in vivo imaging biomarker for

senescent cells could help identify candidates for senolytic therapies and monitor their response to these therapies.

Magnetic resonance imaging (MRI), often enhanced with gadolinium (Gd) chelates as MRI contrast agents is the standard clinical imaging modality for diagnosing degenerative arthritis in patients with OA¹¹. MRI primarily detects downstream sequelae of disease progression, such as osteophytes, cartilage loss, and subchondral cysts¹². These findings reflect structural changes, not directly capturing the underlying molecular drivers of disease progression. Senescent cells are characterized by several markers such as p16, p21, p53, and β -galactosidase (β -gal)^{9,13}.

Bioresponsive MRI contrast agents can be engineered for the detection of β -gal activity¹⁴. We developed a β -gal responsive Gd-chelate with a shielding ligand that can switch T_1 signal on. The coordination sphere of Gd (III) is saturated by a β -galactosyl moiety and bridging ligand before enzyme reaction, preventing the interaction with water protons and resulting in relatively low signal on T_1 -weighted MRI scans. Upon exposure to β -gal, the

¹Molecular Imaging Program at Stanford (MIPS), Department of Radiology, Stanford University School of Medicine, Stanford, CA, 94305, USA. ²Department of Chemistry, Molecular Biosciences, Neurobiology and Radiology, Northwestern University, Evanston, IL, 60208, USA. ³Division of Cardiovascular Medicine, Stanford University School of Medicine, Stanford, CA, 94305, USA. ⁴Department of Radiation Oncology and Medical Physics, Stanford University, Stanford, CA, 94305, USA. ⁵Department of Orthopaedic Surgery, Stanford University, Stanford, CA, 94305, USA. ⁶These authors contributed equally: Kerem Nernekli, Dilyana B. Mangarova, Vidyani Suryadevara. ⁷These authors jointly supervised this work: Thomas J. Meade, Heike E. Daldrup-Link. ✉e-mail: vidyani@stanford.edu; tmeade@northwestern.edu; heiked@stanford.edu

β -galactosyl moiety is cleaved, leading to the release of the bridging ligand and opening the coordination site of Gd (III) for the interaction with water protons, which results in an increased bright (hyperintense) MRI signal on T_1 -weighted MRI scans. Cells that express β -gal cleave the ligand, allowing for improved interaction of the Gd-chelate with protons and a significant boost in the T_1 -signal. This enhanced signal identifies β -gal expressing cells on T_1 -weighted MR images. Taghian et al. reported successful in vivo imaging of β -gal expressing cells with a bioresponsive Gd-chelate in a murine model of GM1-gangliosidosis¹⁵. To our knowledge, nobody has investigated whether β -gal responsive Gd-chelates can be used to detect senescent cells in arthritic joints.

There is currently no diagnostic test available that can detect and quantify β -galactosidase expression by senescent cells in vivo, in articular joints. Thus far, cellular senescence in the joint synovium, articular cartilage, and bone/marrow has been diagnosed ex vivo, based on SA- β -gal activity^{16–19}, cell cycle restricted proteins^{17,18,20} and production of reactive oxygen species, among others, using immunohistochemistry^{18,20}, flow cytometry¹⁷ or fluorescence imaging² approaches. However, none of these previously applied biomarkers is clinically translatable. We hypothesized that a β -gal responsive Gd-chelate might offer a non-invasive MRI method for detecting β -gal expressing senescent cells in porcine knee joints. We opted to implant senescent cells and viable control cells into the joints to allow for a precise correlation between MRI contrast enhancement and the specific location of the cells. The purpose of our study was to evaluate whether our β -gal responsive Gd-chelate can non-invasively detect β -gal expressing senescent cells using MRI in vitro, ex vivo, and in vivo in porcine knee joints.

Results

Optimal concentration of β -gal responsive Gd-chelate

Effective detection of the activation of the β -gal responsive Gd-chelate relies on a narrow concentration window. Excessive Gd-chelate concentrations lead to an overwhelming non-activated signal, while low concentrations limit the detectable activation of the probe and resulting signal enhancement. Figure 1 shows the T_1 -weighted MR contrast effect of β -gal responsive Gd-chelate without and with β -gal enzyme. On T_1 -weighted MR images and T_1 mapping (Fig. 1A and C), test tubes with β -gal responsive Gd-chelate after incubation with β -gal enzyme showed enhanced T_1 contrast effect and shorter T_1 relaxation time (Fig. 1B, Supplementary Fig. 1). The r_1 relaxivity of β -gal responsive Gd-chelate after incubation with β -gal enzyme was higher ($r_1 = 4.9 \text{ mM}^{-1} \text{ s}^{-1}$) compared to β -gal responsive Gd-chelate without incubation with β -gal ($r_1 = 3.3 \text{ mM}^{-1} \text{ s}^{-1}$; Fig. 1D). Additionally, T_2 -weighted MR imaging of test tubes with the β -gal responsive Gd-chelate without and with β -gal enzyme (Supplementary Fig. 2A) indicated higher r_2 relaxivity of β -gal responsive Gd-chelate after incubation with β -gal enzyme ($r_2 = 5.0 \text{ mM}^{-1} \text{ s}^{-1}$) compared to β -gal responsive Gd-chelate without β -gal ($r_2 = 3.2 \text{ mM}^{-1} \text{ s}^{-1}$; Supplementary Fig. 2B).

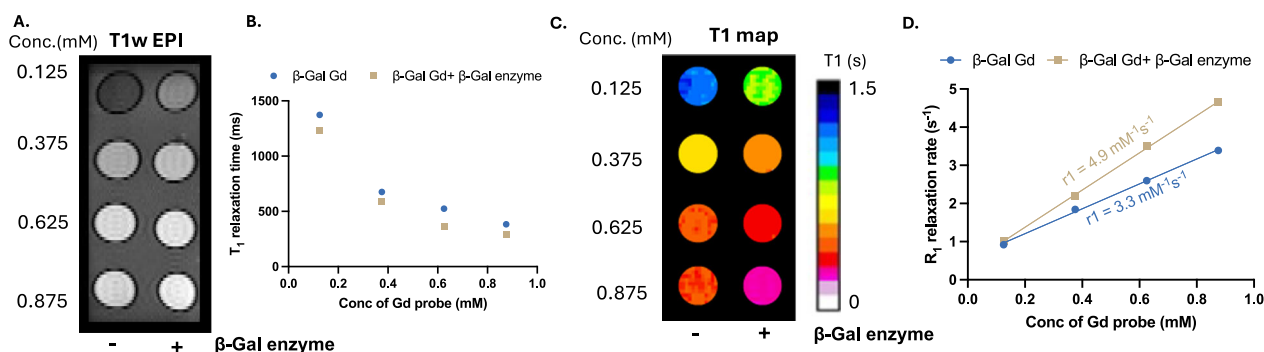


Fig. 1 | Determining the optimal concentration of the β -gal responsive Gd-chelate for MRI detection of β -gal Gd-chelate 'activation'. A Representative axial T_1 -weighted MR images of test tubes with increasing concentrations of the β -gal responsive Gd-chelate, with and without the addition of 10U β -gal enzyme at pH 6.0. **B** Mean T_1 relaxation times of increasing concentrations of the β -gal responsive Gd-

MRI differentiation of senescent and viable cells with the β -gal responsive Gd-chelate

To assess the ability of the β -gal responsive Gd-chelate to discriminate viable and senescent mesenchymal stromal cells (MSCs), we incubated MSC with the Gd-chelate, followed by MRI analysis. Triplicate samples of 1×10^7 primary MSCs were incubated with doxorubicin, a senescence inducer²¹. $89 \pm 2.1\%$ of these cells were β -gal positive compared to $13 \pm 3.2\%$ untreated controls ($p = 0.025$) (Fig. 2A and B). The SASP phenotype of doxorubicin-exposed cells was further confirmed by an increase in the expression levels of IL-6 (control: $490 \pm 75 \text{ pg/mL}$, senescence: $2700 \pm 160 \text{ pg/mL}$, $p = 0.025$) and IL-8 (control: $1100 \pm 46 \text{ pg/mL}$, senescence $2600 \pm 240 \text{ pg/mL}$, $p = 0.025$) (Fig. 2C). Additional markers which indicate cell cycle arrest²² were used to confirm doxorubicin-induced senescence, as seen by increased p53 (3.43 fold change, $p = 0.014$, Fig. 2D and E), increased p21 (2.08 fold change, $p = 0.014$, Fig. 2D and E) and reduced Lamin B1 (0.68 fold change, $p = 0.014$, 3D, 3E) protein expression in senescent cells compared to control cells, as determined by western blotting (Fig. 2D and E). Viable and senescence MSCs treated with β -gal responsive Gd-chelate had no effect on the viability, as determined by CCK-8 assay (Fig. 2F). Senescent MSCs exposed to β -gal responsive Gd-chelate at 0.5 and 0.25 mM exhibited a mean R_1 relaxation rate of 3.7 ± 0.43 and $3.1 \pm 0.51 \text{ s}^{-1}$, respectively (Fig. 2G). Viable MSCs exposed to β -gal responsive Gd-chelate at the 0.5 and 0.25 mM concentrations showed a mean R_1 relaxation rate of 2.0 ± 0.73 and $1.6 \pm 3.1 \text{ s}^{-1}$, respectively. At 0.5 mM concentration, senescent cells demonstrated stronger MRI signal on T_1 -weighted MRI images and significantly longer R_1 relaxation rates compared to viable controls ($N = 9$; 0.25 mM, $p = 0.084$; 0.5 mM, $p = 0.013$) (Fig. 2H). ICP-OES measurements of the same cell samples demonstrated no significant difference in Gd concentration of control and senescent cell samples exposed to β -gal responsive Gd-chelate (Fig. 2I), indicating that the increased T_1 -signal of senescent cells is due to activation of the β -gal responsive Gd-chelate.

β -gal responsive Gd-chelate detects senescent cells in pig knee specimens with MRI

To assess the ability of β -gal responsive Gd-chelate to detect senescent cells against the typical anatomical background tissue of an articular joint, we incubated control and senescent cells with the Gd-chelate and implanted them into cartilage defects of pig knee specimen, followed by MRI. T_1 -weighted spin-echo (T_1 -SE) sequences provided anatomical details, while a T_1 -weighted RARE variable TR saturation recovery sequence was used to generate T_1 maps for quantitative R_1 relaxation rate measurements. Implants of senescent MSCs exhibited a more pronounced hyperintense signal on T_1 -weighted MR images compared to their viable counterparts (Fig. 3A). The mean R_1 relaxation rate of senescent cell implants ($1.6 \pm 0.80 \text{ s}^{-1}$) was significantly longer than the R_1 relaxation rate of viable cell implants ($0.97 \pm 0.27 \text{ s}^{-1}$; $p = 0.007$) (Fig. 3B). Accordingly, the signal-to-noise ratio

chelate with and without the addition of 10U β -gal enzyme. **C** Corresponding T_1 maps are color-coded to depict T_1 -shortening visually. **D** Mean R_1 relaxation rates of increasing concentrations of the β -gal responsive Gd-chelate with and without the addition of 10U β -gal enzyme.

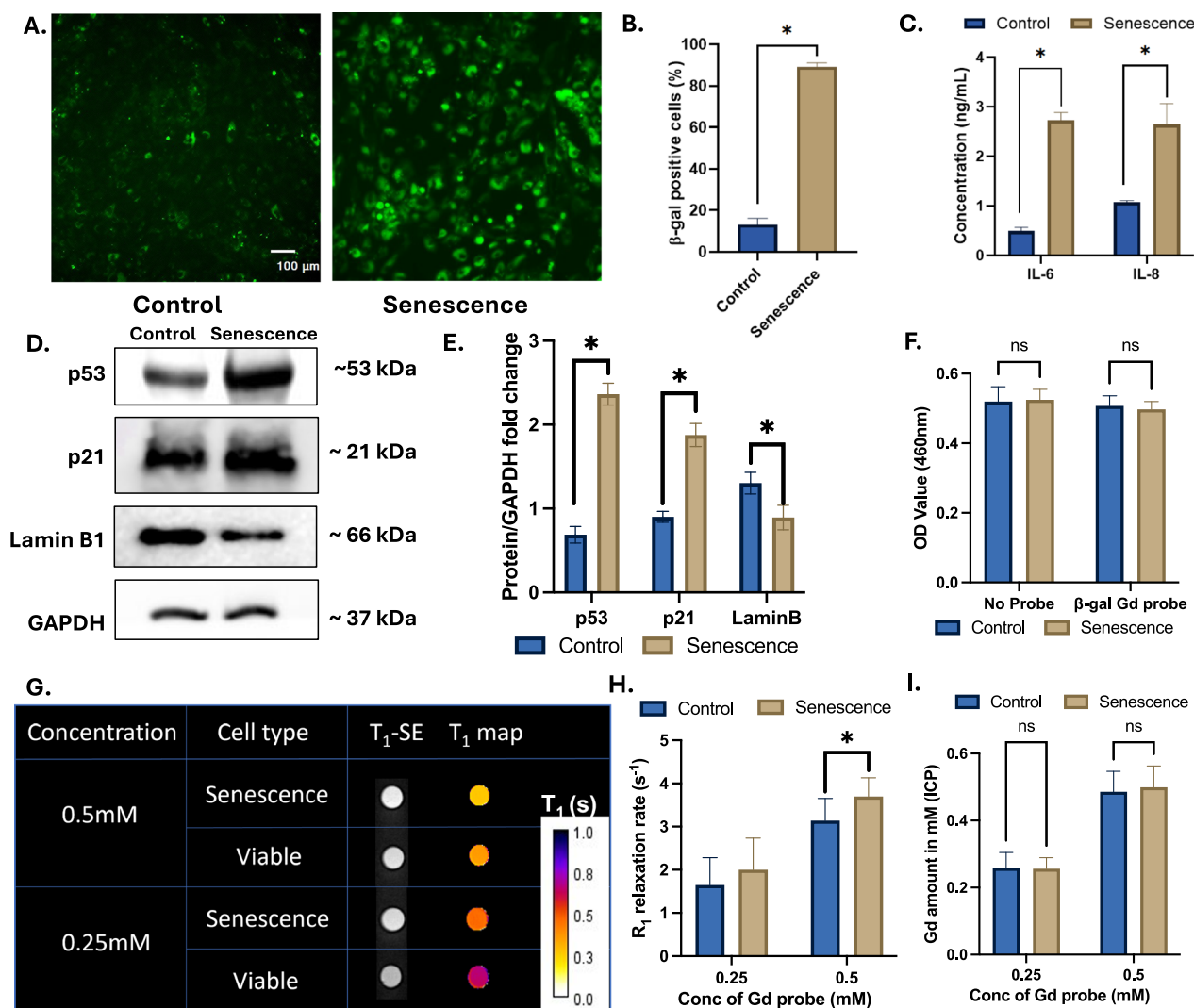
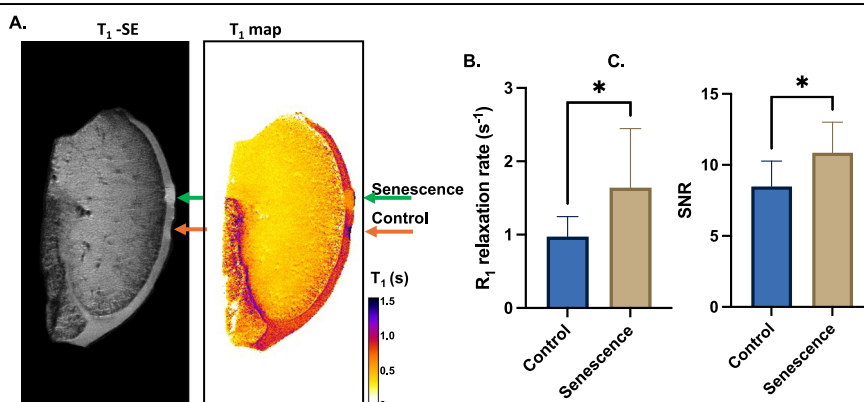


Fig. 2 | Senescence of MSCs detected by β-gal responsive Gd-chelate. **A** Confocal microscopy of senescent and viable mesenchymal stromal cells (MSC) after incubation with CellEvent™ Senescence Green Probe. Green fluorescence indicates β-gal expression. **B** Relative number of β-gal positive green fluorescent cells (%) for senescent MSC and viable control MSC on fluorescence microscopy with CellEvent™ Senescence Green staining. **C** IL-6 and IL-8 levels of control and senescent cells, as measured with ELISA. **D** Western blots depicting p53, p21, and Lamin B1 expression in control and senescent cells along with loading control GAPDH. **E** Band intensities of p53, p21, and Lamin B1 were quantified and normalized to GAPDH with ImageJ software. **F** CCK-8 assay to indicate the viability of control and senescent cells with and without incubation with the β-gal responsive Gd-chelate. **G** Representative axial

T₁-weighted MR images acquired on a 3 T MRI of test tubes with senescent cells or viable controls after incubation with different concentrations of the β-gal responsive Gd-chelate. Corresponding T₁ maps are color-coded to depict T₁-shortening. **H** Quantitative R₁ relaxation rates, derived from T₁ maps, of control and senescent MSCs after incubation with 0.25 and 0.5 mM β-gal responsive Gd-chelate. **I** ICP-OES measurements demonstrated no significant difference in Gd concentration of test tubes with β-gal probe with added viable or senescent MSC, confirming that the concentration of the probes did not change significantly after addition of cells. Therefore, changes in MRI signal are due to activation of the probe. Data are displayed as means and standard deviations of ten samples per experimental group. **p* < 0.05.

Fig. 3 | Senescent cells in porcine explants detected by β-gal responsive Gd-chelate. **A** Representative sagittal T₁-weighted MR image acquired on a 3 T MRI of a distal femur specimen with implants of senescent cells (green arrow) and viable cells (orange arrow) in full-thickness cartilage defects and corresponding T₁ map. **B** Corresponding mean R₁ relaxation rates of senescent cell implants and controls. **C** Mean Signal-to-noise ratios of senescent cell implants and controls. All data are displayed as means and standard deviations of ten implants per group. **p* < 0.05.



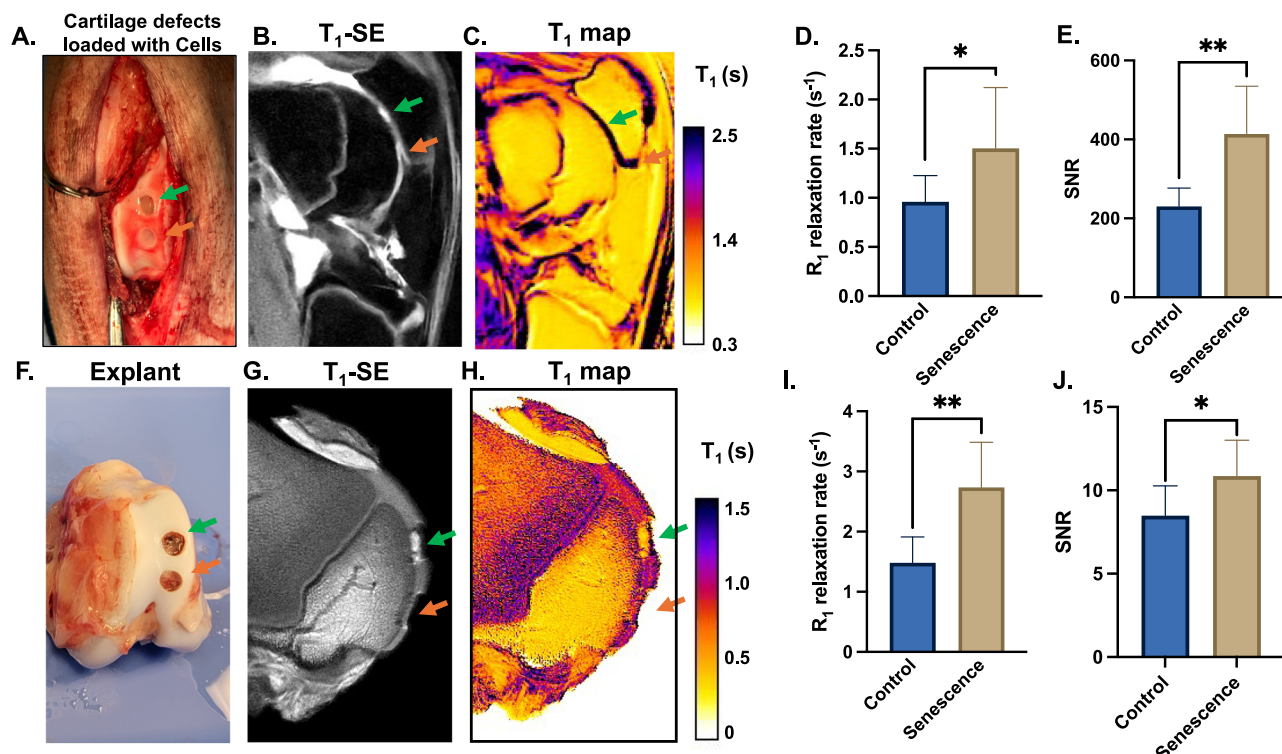


Fig. 4 | Detection of senescent cells with the β -gal responsive Gd-chelate and MRI.

A Intraoperative photo of cartilage defects in the distal femur of a live pig with implants of senescent cells (green arrow) and viable cells (orange arrow). **B** Representative sagittal T_1 -weighted MR image acquired on a 3 T MRI of the same knee joint after intra-articular injection of the β -gal responsive Gd-chelate. Senescent cells (green arrow) demonstrate stronger T_1 -signal compared to viable cells (orange arrow). **C** Corresponding T_1 map demonstrates T_1 -shortening in senescent cells (green arrow) compared to viable cells (orange arrow). **D** Corresponding mean R_1 relaxation rates of senescent cell implants and viable cell implants. **E** Mean signal-to-noise ratios (SNR) of senescent cell implants and viable cell implants. **F** Photo of

excised distal femur shows cartilage defects with implants of senescent cells (green arrow) and viable cells (orange arrow). **G** Representative sagittal T_1 -weighted MR image of the explant acquired on a 3 T MRI with senescent cells (green arrow) and viable cells (orange arrow) in full-thickness cartilage defects. **H** Corresponding T_1 map demonstrates T_1 -shortening of senescent cells (green arrow) and not viable cells (orange arrow). **I** Mean R_1 relaxation rates of implants with senescent cells and control cells. **J** SNR values for implants with senescent cells and control cells. Data are displayed as means and standard deviations of eight implants per experimental group. * $p < 0.05$, ** $p < 0.005$.

(SNR) of senescent cell implants (SNR: 11 ± 2.1) was significantly higher compared to viable controls (SNR: 8.5 ± 1.8 , $p = 0.032$) (Fig. 3C).

β -gal responsive Gd-chelate detects senescent cells in vivo with MRI

We next evaluated the ability of the β -gal responsive Gd-chelate to detect senescence in vivo in the knee joints of live pigs using MRI. We implanted 1×10^7 senescent and 1×10^7 control cells into full-thickness cartilage defects of eight distal femurs of four Yucatan minipigs (Fig. 4A). 24 h later, we injected 5 ml of 2.5 mM β -gal responsive Gd-chelate intraarticularly into each knee joint. The higher concentration compared to in vitro studies was chosen to account for the dilution of our probe in joint fluid. T_1 -weighted MRI scans after intra-articular injection of the β -gal responsive Gd-chelate revealed stronger MRI signal in cartilage defects containing senescent cells compared to defects with control cells (Fig. 4B and C). The R_1 relaxation rate calculated from the T_1 maps indicated significant activation of the β -gal responsive Gd-chelate in senescent cell implants ($1.5 \pm 0.61 \text{ s}^{-1}$) compared to controls ($0.95 \pm 0.26 \text{ s}^{-1}$, $p = 0.01$) (Fig. 4D). Accordingly, the signal-to-noise ratio (SNR) of senescent cells (SNR: 410 ± 120) was significantly higher compared to that of control viable cells (SNR: 230 ± 47 ; $p = 0.001$) (Fig. 4E). To further demonstrate the specific activation of senescent cells loaded in the cartilage defects, we performed MRI of the knee joint prior to intra-articular injection of the β -gal responsive Gd-chelate and found no bright signal in the cartilage defect loaded with senescent cells, in contrast to the bright signal in the sagittal T_1 -weighted MR image of the same knee joint at 2 h after intra-articular injection of the β -gal responsive Gd-chelate (Supplementary Fig. 3).

After sacrificing the animal, the knee joints were excised (Fig. 4F) and underwent ex vivo MR imaging. Similar to the results in live pigs, implants of senescent MSCs exhibited a more pronounced hyperintense signal on T_1 -weighted MR images compared to their viable counterparts (Fig. 4G and H). The R_1 relaxation rate of senescent cell implants ($2.7 \pm 0.75 \text{ s}^{-1}$) was significantly higher compared to viable cell implants ($1.5 \pm 0.42 \text{ s}^{-1}$; $p = 0.002$) (Fig. 4I). Furthermore, the signal-to-noise ratio (SNR) of the MRI signal was significantly higher for senescent cells (11 ± 2.0) compared to controls (8.5 ± 1.7 ; $p = 0.018$) (Fig. 4J). Taken together, results indicate that the β -gal responsive Gd-chelate exhibits potential as an MR probe for imaging senescent cells in articular joints.

Validation of senescence MR imaging with immunocytochemistry

To further confirm our new imaging technique with established methods for detecting senescent cells, we performed histological analysis of all pig knee specimens. We employed immunocytochemistry (ICC) to visualize additional senescence markers, including p16, p21, and β -gal. We found that senescent cell implants in cartilage defects expressed significantly higher levels of p16 (Control: 277.00 ± 51.06 , Senescence: 3000 ± 290) (Fig. 5A and D), p21 (Control: 170 ± 25 , Senescence: 2800 ± 27) (Fig. 5B and D) and β -gal (Control: 200 ± 25.31 , Senescence: 2900 ± 280) (Fig. 5C and D) compared to control implants ($p = 0.025$). This sustained expression of senescence markers indicates that implanted cells retained their characteristic features throughout the duration of our experiment. We performed additional staining to confirm the presence of MSCs in the cartilage defects one day after implantation of the cells and that the differences in R_1 relaxation times

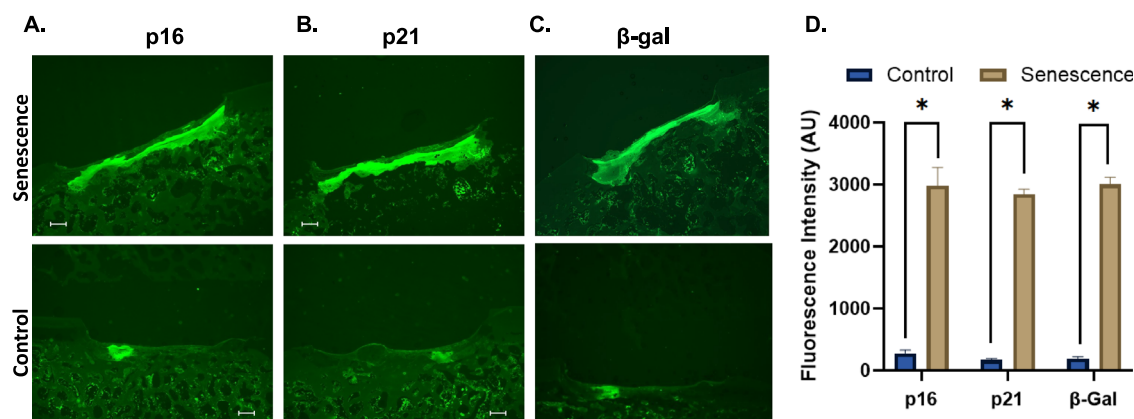


Fig. 5 | Histological comparison of viable and senescent cell implants in pig knee cartilage. After MRI, the pig knee joints were excised and processed for histology. Fluorescence images of cartilage defects with implants of senescent cells and viable control cells, stained with (A) p16 ($\times 2$ magnification), (B) p21 ($\times 2$ magnification), and (C) β -gal ($\times 2$ magnification). D Fluorescence intensity of senescent cells and viable controls on respective stains. All data are displayed as mean data and standard deviations of eight implants per group. * $p < 0.05$.

are due to the distinct differences between control and senescent cells and not an influx of macrophages or variance in vascularity. The retention of MSCs in the cartilage defects of pig knees on day 2 was confirmed by the expression of CD73²³, CD90, and CD105 in the cartilage defects loaded with control and senescent cells (Supplementary Fig. 6). CD73, CD90, and CD105 are well-established surface markers of mesenchymal stem cells. Further, trichrome staining which stains the collagen fibers blue, indicated no fibrosis in the cartilage defects (Supplementary Fig. 7). F4/80 staining indicates no difference in the influx of macrophages in the defects loaded with control and senescent cells (Supplementary Fig. 8A). F4/80 is a well-established cell-surface marker for macrophages²⁴. The quantification of immunofluorescence staining was done as described previously²⁵. CD31 staining indicates no vascularity in the defects loaded with control and senescent cells (Supplementary Fig. 8B).

Discussion

This study demonstrated that a β -gal responsive Gd-chelate can detect senescent cells non-invasively using MRI in vitro, in knee explants, and in vivo, in a live pig model. Our senescence induction model yielded a robust senescence phenotype, as confirmed by established biomarkers, including increased levels of senescence-associated β -gal (SA- β -gal), IL-6, and IL-8, as described by Muñoz-Espín et al.²⁶. Currently, the most widely used biomarker for identifying senescent cells in vitro and in vivo is SA- β -gal activity²⁷. Senescent cells overexpress the GLB1 gene, which leads to SA- β -gal production, lysosomal storage, and secretion¹³.

Several investigators used other imaging techniques such as bioluminescence imaging or fluorescence imaging to detect SA- β -gal in vitro and in vivo. Yang L. et al. used a methylene blue (MB) fluorophore coupled to β -galactose (MB- β -gal) to detect senescent HeLa cells and mouse embryonic fibroblast (MEF) cells in vitro. Upon exposure to β -gal, MB- β -gal released free methylene blue (MB), generating near-infrared (NIR) fluorescence detectable with optical imaging techniques²⁸. Redy-Keisar, O. et al. described the GQCy7 compound, which undergoes a chemical reaction where the glycosidic bond is hydrolyzed when exposed to β -gal. The release of QCy7 resulted in an extended π -conjugated system that underwent an internal charge transfer process, turning the fluorescence “on.” Mice injected with a solution of GQCy7 that had been incubated with β -gal showed an increased near-infrared fluorescent (NIR-fluorescent) signal²⁹. Wehrman, T. et al. developed a bioluminescent imaging approach that allowed for noninvasive in vivo imaging of β -galactosidase activity. In their study, in vitro and in vivo experiments were performed to test Lugal, a caged luciferin-galactoside conjugate, which is cleaved by β -galactosidase to produce luminescence³⁰. Lee H.W. et al. developed a fluorescent biomarker, which showed a blue-to-yellow color change in response to β -gal. They used this fluorescent probe to

detect senescence-associated β -gal in murine fibroblast skin cells and rat skin tissue in vitro using two-photon microscopy³¹.

While previous studies targeting β -gal for senescence detection have demonstrated promise, their reliance on fluorescence³² and optical imaging restricts their application to preclinical models due to the limited tissue penetration of the applied imaging biomarker³³. This hinders clinical translation. To overcome this limitation, we used MR imaging, the gold standard for clinical imaging of OA in knee joints. The MR contrast effect of Gd(III) can be modulated through various physical parameters, such as the number of bound water molecules (q), the rate of molecular tumbling (τ_r), and the rate of water exchange (τ_m)³⁴. Louie, A. et al. described that a q modulation octadentate Gd(III) chelate has one coordination site for water exchange which can be activated in the presence of β -galactosidase³⁵. Lilley et al. showed that adjusting the molecule’s overall size and shape can improve the molecules’ response to β -gal³⁴. Our team added a pendent carboxyl ligand, which can saturate the coordination sphere of Gd(III). This led to significant signal differences between the inactive (“off”) and active (“on”) versions of the probe, enabling us to effectively detect senescent cells in vitro and in vivo. We have previously demonstrated in vivo experiments in wild-type mice and transgenic mice which express LacZ that encodes the β -gal enzyme in visceral organs. The transgenic mice demonstrated strong hyperintense signal enhancement of the liver, spleen, and kidneys on T_1 -weighted MRI after intravenous injection of the SA- β -Gal-sensitive Gd-probe, unlike native control mice³⁴.

We recognize several limitations of our study. Due to its close resemblance to human joints in both anatomy and physiology, the pig model is frequently used to represent human cartilage injuries³⁶. There is no established large animal model for the detection of senescent cells in cartilage defects to our knowledge. We implanted either senescent or viable mesenchymal stem cells (MSCs) into cartilage defects of porcine knee joints. 24 h later, we conducted an MRI arthrography using the β -galactosidase-responsive Gd-chelate. While this experimental design enabled precise colocalization of MRI contrast enhancement with the known presence of senescent cells, it does not fully capture the complexities of the naturally occurring environment found in degenerative OA or inflammatory arthritis. While several investigators described the central role of senescent cells in the pathogenesis of osteoarthritis^{37,38}, further studies are needed to determine the sensitivity and specificity of our probe in affected patients.

For our specific application of detecting senescent cells in arthritic joints with the β -gal responsive Gd-chelate, we followed the established procedure for MRI arthrograms in clinical practice³¹. Previous studies have been conducted after intrathecal and intraperitoneal injection of β -gal responsive Gd-chelate in mouse models of GM1-gangliosidosis¹⁵. Taghian et al. reported a statistically significant enhancement of β -gal activity of the

brain at 110 min after intrathecal injection of 0.06 mol/kg of the β -gal responsive Gd-chelate¹⁵. This study reported longitudinal probe dynamics in vivo after intrathecal injection, revealing a peak enhancement of the brain at 40 min, followed by a steady state for at least 110 min. Based on this data, we selected a time window of 1–2 h post-intraarticular injection for our investigation of β -galactosidase activity in articular cartilage. In future studies, investigating longitudinal MRI at multiple time points after intra-articular injection of the β -galactosidase-responsive Gd-chelate could yield additional insights into the probe's biodistribution and help identify optimal imaging windows. Ultimately, for clinical applications, a single imaging session would be required.

Our in vitro studies employed doxorubicin to induce cellular senescence, as confirmed by the presence of established senescence markers. The senescent cells, and not the non-treated control cells, expressed β -galactosidase. In this controlled experimental setting, there were no other sources of β -galactosidase. Therefore, our data supports the conclusion that the senescent cells produced β -galactosidase, and that our β -gal-sensitive contrast agent detected β -galactosidase expression by senescent cells. We did not quantify intracellular Gd-uptake by the cells using ICP-MS or similar methods. Therefore, it is unclear if our β -galactosidase responsive Gd-chelate detected intracellular or extracellular β -galactosidase.

β -galactosidase is produced by lysosomes within the cells. Duan et al. reported that LakZ expressing *Bacillus subtilis* bacteria excrete approximately 65% into the extracellular space³⁹. We did not measure the relative proportion of intra- and extracellular β -galactosidase in MSCs in our study. Clinical Gd-chelates distribute primarily in the intravascular and extracellular space, with little or no intracellular contrast agent accumulation⁴⁰. However, MSC can take up Gd-chelates after incubation with the probe⁴¹, a condition that reflects our MR arthrography setting. Therefore, it is probable that the observed MRI signal reflects a combination of intracellular and extracellular contrast agent activation, though extracellular Gd-chelate, with its higher concentration and effective relaxivity, likely plays a more significant role. Several investigators reported that small molecular Gd-chelates exhibit reduced effective relaxivity after being internalized into cells, likely due to limited interactions with water protons^{42,43}. Further studies are needed to clarify the relative contributions of extracellular and intracellular β -galactosidase to the activation of the β -galactosidase responsive Gd-chelate and the observed MRI signal.

When using histology and immunohistochemistry, detection of senescent cells involves the use of multiple senescent-specific markers such as p16 and p21 with β -gal⁴⁴. Accordingly, further developments of our β -gal responsive Gd-chelate could involve dual-modality approaches to enhance its specificity. We are currently working on ¹⁸F-labeled versions of our biomarker for simultaneous detection of β -gal expression with MRI and positron emission tomography (PET). Future studies could combine our β -gal responsive Gd-chelate with a radiotracer or fluorophore for the detection of a different biomarker of senescence, such as p16 or p21.

We anticipate broad applicability for our approach. In addition to osteoarthritis, senescence plays an important role in embryonic development⁴⁵, atherosclerosis⁴⁶, cardiomyopathy⁴⁷, cancer⁴⁸, pulmonary fibrosis⁴⁹, and neurodegenerative disorders⁵⁰, among others. Our β -gal responsive Gd-chelate holds promise for: (1) quantifying and mapping the biodistribution of senescent cells in these diverse conditions, (2) elucidating risk factors that exacerbate senescence development, and (3) exploring whether senescence differs between patients with varying genetic or ethnic/racial backgrounds. In addition, our β -gal responsive Gd-chelate might be useful for monitoring new senolytic therapies. Novais et al. explored the ability of Dastinib and Quercetin drug combination (D + Q) to reduce intervertebral disc degeneration in mice⁵¹. Baker et al. designed a new transgene, INK-ATTAC for selective elimination of p-16-positive senescent cells in mice³⁷. Cai et al. developed a prodrug strategy wherein they designed SSK1, which cleared senescent cells in different tissues⁵². Considering the clinical translation of several senolytic drugs for the treatment of osteoarthritis, further studies exploring the

effects of senolytic therapies on the MR imaging signal of arthritis joints are crucial and hold significant potential to advance our understanding and treatment of osteoarthritis.

A major advantage of our β -gal responsive Gd-chelate is that it can be applied repeatedly in the same subject, to evaluate changes in senescent cell distribution or quantity over time. Our imaging technique is not associated with any irradiation and exposure and can easily be integrated with clinical standard MRI protocols. Future studies have to show if our probe can detect changes in senescence-related diseases on longitudinal imaging studies. Additionally, the successful translation of our probe to first-in-human clinical trials will require biodistribution studies and comprehensive toxicology tests. Our β -gal responsive Gd-chelate could be used to select patients with a high burden of senescent cells, prescribe tailored treatment strategies, and monitor response to these therapies, ultimately decelerating disease progression and enhancing the quality of life for patients with OA and other age-related disorders.

In conclusion, we introduced a new β -gal responsive Gd-chelate for detecting senescent cells in porcine knee joints on MR images. Upon validation in clinical osteoarthritis, this new β -gal responsive Gd-chelate has the potential to aid in diagnosing senescence linked to natural aging and degenerative joint diseases. It could also serve as a new clinically translatable biomarker for monitoring the effectiveness of new therapies designed to eliminate senescent cells (senolytics).

Methods

Characterization of β -gal responsive Gd-chelate

Our β -gal responsive biomarker is composed of a Gd-chelate and a pendant coordinating carboxylate unit connected via a six-carbon (C6) linker to an aniline moiety (Fig. 6). Prior to enzyme activation, the Gd (III) coordination sphere is fully occupied by the β -galactosyl moiety and a bridging ligand, blocking interaction with water protons. This translates to a weak signal on T_1 -weighted MRI scans. Exposure to β -gal triggers cleavage of the β -galactosyl moiety, releasing the bridging ligand and exposing a coordination site on Gd (III). This newly accessible site permits interaction with water protons, resulting in a strong signal enhancement on T_1 -weighted MRI scans³⁴.

The chemical structure of our β -gal responsive Gd-chelate is shown in Fig. 6. It has a molecular weight of 986 Da. The r_1 relaxivity of the probe in the absence of β -gal is $3.2 \text{ mM}^{-1} \text{ s}^{-1}$ at 1.41 T and 37 °C and the r_1 relaxivity of the probe in the presence of β -gal is $3.91 \text{ mM}^{-1} \text{ s}^{-1}$ at 1.41 T and 37 °C (Supplementary material: Fig. 4A, Table 1). The r_2 relaxivity of the probe in the absence of β -gal is $3.16 \text{ mM}^{-1} \text{ s}^{-1}$ at 1.41 T and 37 °C and the r_2 relaxivity of the probe in the presence of β -gal is $4.08 \text{ mM}^{-1} \text{ s}^{-1}$ at 1.41 T and 37 °C (Supplementary material: Fig. 4B, Table 1). The relaxivity at 1.41 T was measured by scanning increasing concentrations of 0.23, 0.33, 0.47, 0.65, and 0.84 mM of the β -gal responsive Gd-chelate, with and without the addition of 17U β -gal at pH 6.0. Suppl. Fig. 5 shows R1 relaxation rate measurements in vitro, assessing test-retest and inter-reader agreement within each group (senescent-senescent and viable-viable) to confirm reproducibility of R1 measurements.

The r_1 relaxivity of the probe in the absence of β -gal is $3.9 \text{ mM}^{-1} \text{ s}^{-1}$ at 3 T and 37 °C and the r_1 relaxivity of the probe in the presence of β -gal is $4.7 \text{ mM}^{-1} \text{ s}^{-1}$ at 3 T and 25 °C. The relaxivity was measured by scanning increasing concentrations of 0.125, 0.25, 0.5, 0.625, 0.75 and 1 mM of the β -gal responsive Gd-chelate, with and without the addition of 10U β -gal at pH 6.0. The relaxivity at 3 T was measured by standard linear fitting of the R_1 relaxation rate measurements at different concentrations of the β -gal responsive Gd-chelate. Simple linear regression analysis was used for linear fitting of the relaxation rate versus concentrations and calculated by $y = \alpha + \beta \cdot x$.

Induction of senescence in MSCs, as confirmed by ELISA and β -gal assays

Bone marrow-derived MSCs were isolated from 10 ml of bone marrow fluid aspirated from the iliac crest of donor pigs using established techniques⁵³.

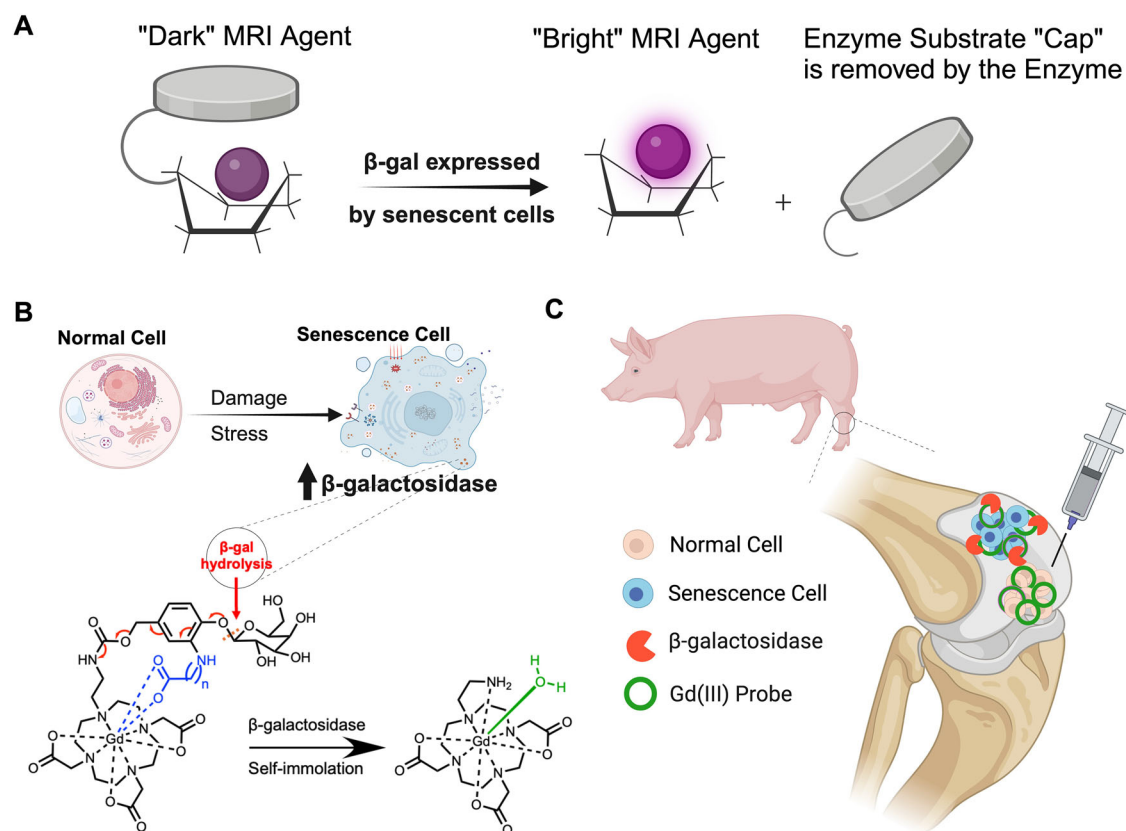


Fig. 6 | Concept of imaging senescent cells with a β -gal sensitive Gd-chelate.

A Concept of β -Gal activation by cleavage of a pendant carboxylate ligand. The β -Gal-activated MR probe is composed of gadolinium (Gd III) conjugated to a hydrophilic β -Gal substrate. Before enzyme reaction, the coordination sphere of Gd is saturated by a β -galactosyl moiety and a bridging ligand, preventing the interaction with water protons and resulting in low signal on T₁-weighted MRI scans. After exposure to β -gal, the β -galactosyl moiety is cleaved, opening the coordination site of Gd III for proton interaction and resulting in an increased (hyperintense) MRI signal on T₁-weighted MR scans. **B** Molecular changes of β -gal sensitive Gd-chelate after

exposure to β -gal. Upon stress/damage, cells in the joint compartment undergo senescence, resulting in the expression of β -gal. Before activation by β -gal, the β -galactosyl moiety (blue) of the Gd-chelate prohibits water access to Gd (III). After exposure to β -gal, the β -galactosyl moiety is cleaved and an electron cascade (red) provides an open coordination site for water to bind to Gd (III). **C** Study design. Viable or senescent mesenchymal stromal cells were implanted in cartilage defects of the distal femur of pig knee joints. The β -gal responsive Gd-chelate was injected into the knee joint, leading to activation of the β -gal sensitive Gd-chelate in senescent cell transplants and not viable cell transplants, as measured by MRI.

The cells were cultured in Dulbecco's modified Eagle medium (DMEM) containing 1% penicillin–streptomycin (pen-strep) and 10% fetal bovine serum (FBS) at 5% CO₂ and 37 °C. The media was replenished every 24–48 h. After reaching ~90% confluency, adherent MSCs were further expanded, used for experiments, or stocked at –195 °C. MSCs were used at a low passage number ($p = 3$ or $p = 4$) to avoid spontaneous senescence.

Triplicate samples of 1×10^7 MSCs in 12-well plates in DMEM media were exposed to 400 nM doxorubicin on day 1 and day 3, followed by analysis for senescence on day 5. Triplicate samples of 1×10^7 MSCs in DMEM media served as non-exposed controls. Control and senescent cells were washed with phosphate-buffered saline (PBS) twice and fixed with 2% paraformaldehyde in PBS for 10 min at room temperature. The fixative solution was removed by washing the cells thrice with 1% bovine serum albumin (BSA) in PBS. Cells were stained for senescence detection using the Senescence Green Probe from the CellEvent Senescence Green Detection Kit (C10851, Invitrogen). Briefly, the probe was warmed to 37 °C for 10 min in the dark before being added to the cells for a 2-h incubation at 37 °C without CO₂ and under dark conditions. Following incubation, cells were washed three times with PBS and then imaged using a fluorescent microscope (Keyence, BZ-X710, Cupertino, CA).

In addition, the supernatants were collected for ELISA analysis. Commercially available kits were used to measure IL-6 (RAB0310, Sigma, St. Louis, MA) and IL-8 (RAB0321, Sigma, St. Louis, MA) levels in the supernatants, as per the manufacturer's instructions.

Western blotting

Lysates from control and senescent cells were subjected to SDS-PAGE on a 10% or 4–20% precast gel (Invitrogen, Carlsbad, CA) run at constant voltage (225 V) and transferred to nitrocellulose membranes (Bio-Rad, Hercules, CA). The membrane was blocked for 1 h at room temperature in blocking buffer [Tris-buffered saline + Tween 20 (TBST) with 1% BSA] to reduce nonspecific binding. The membranes were then incubated with the respective primary antibodies overnight. All primary antibodies used were either validated by the supplier or in our laboratory. The primary antibodies used were LaminB (no. 13435, 1:1000 dilution; Cell Signaling), p21 (no. ab188224, 1:1000 dilution; Abcam), and p53 (no. 9282, 1:1000 dilution; Cell Signaling); GAPDH (1:10,000 dilution, no. 5174, Cell Signaling). After four 10-min washes with TBST, membranes were incubated for 1 h with the respective species-specific horseradish peroxidase-conjugated secondary antibodies (Bio-Rad, Hercules, CA) in TBST containing 1% BSA. The membranes were rinsed again four times with TBST for 10 min each time, and bands were detected using Supersignal luminol enhancer (Perbio Science UK, Cheshire, UK) followed by exposure to blue light-sensitive X-ray film (Hyperfilm; Amersham Biosciences, Little Chalfont, UK). Equal protein loading was verified by reprobing membranes with anti- β -actin antibody. The relative intensities of protein bands (relative density units) were quantified by scanning densitometry using ImageJ software (Molecular Dynamics, Sunnyvale, CA).

Determining the optimal incubation time and concentration of the β -gal responsive Gd-chelate

To determine the optimal concentration of the Gd-chelate for the detection of β -gal-mediated MRI signal changes, decreasing concentrations of 1, 0.75, 0.625, 0.5, 0.25, and 0.125 mM β -gal responsive Gd-chelate were suspended in PBS (25 °C, pH 7.4). In a pilot study, we doubled the initial concentration from 0.125 to 0.25, 0.5 and 1 mM. Since 0.25 and 0.5 provided the best results, we repeated the experiment with additional concentrations between 0.5 and 1 mM. One series of samples was left untreated, and a second series was incubated with 10 units of β -gal enzyme (Sigma-Aldrich, St. Louis, MO) at 37 °C for 8 h. To determine the optimal incubation time of the Gd-chelate for the detection of β -gal-mediated MRI signal changes, nine test tubes with 0.5 mM β -gal responsive Gd-chelate were prepared with the addition of 10 mM phosphate buffered saline or with the addition of 17 U of β -galactosidase. All samples underwent T_1 relaxation time measurements at pH 7.4, 37 °C, and 1.7 T, at 10, 20, 30, 40, 60, 80, 120, and 150 min after incubation with either PBS or β -galactosidase. To minimize air-induced artifacts, triplicate samples of the aforementioned solutions in Eppendorf tubes were submerged in water baths before acquiring MRI images. All samples underwent MRI on a 3 T MRI scanner (Bruker BioSpec, Billerica, MA) using a T_1 -weighted sequence (TR = 12,115 ms, TE = 24 ms, FOV = 40 mm \times 20 mm, matrix = 96 \times 64, slice thickness = 1 mm, GLB image size = 96 mm \times 96 mm); inversion recovery sequence (TI = 35–10,000 ms, TR = 11,050–21,015 ms, TE = 24 ms, FOV = 40 mm \times 20 mm, matrix = 96 \times 64, slice thickness = 1 mm, image size = 96 mm \times 96 mm) and T_2 -weighted multi-slice multi-echo sequence (MSME): TR: 3000 ms, TE: 132 ms, slice thickness = 1 mm, FOV = 35 mm \times 35 mm, matrix = 160 \times 160.

MRI differentiation of senescent and viable cells with the β -gal responsive Gd-chelate

Triplicate samples of 1×10^7 MSCs in T-75 flasks in DMEM media were exposed to 400 nM doxorubicin on day 1 and day 3, followed by analysis for senescence on day 5. Triplicate samples of 1×10^7 MSCs in T-75 flasks in DMEM media served as non-exposed controls. Control and senescent cells were washed with phosphate-buffered saline (PBS) twice and trypsinized to obtain cell suspensions. Cell suspensions of triplicate samples of 1×10^7 control and senescent cells were incubated with 0.5 mM or 0.25 mM β -gal responsive Gd-chelate in PBS at 37 °C for 8 h. After the incubation with the β -gal responsive Gd-chelate, the cells were pipetted well to resuspend the cells to obtain a suspension for MRI. All samples underwent MRI on a 3 T MRI scanner (Bruker BioSpec, Billerica, MA), using a T_1 -weighted fast SE sequence for anatomical orientation (repetition time [TR] = 700, time to echo [TE] = 12 ms, 80 mm \times 40 mm field of view [FOV], 192 \times 192-pixel matrix, 12 averages) and a variable TR rapid acquisition with relaxation enhancement (RARE) sequence (TE = 10 ms, TR = 40, 75, 150, 300, 500, 700, 1000, 1500, and 2000 ms, RARE factor = 2, 80 mm \times 40 mm FOV, 500 \times 250 pixel matrix, 2 averages) for generating T_1 -maps and measuring R_1 relaxation rates.

Cell viability assay

To assess the impact of the incubation of the cells with 0.25 and 0.5 mM β -gal responsive Gd-chelate for 24 h, we performed a viability assay, using a commercially available cell Counting Kit 8 (WST-8) (ab228554, Abcam, Cambridge, UK). The cells were seeded in 96-well plate and incubated with 0.5 or 0.25 mM β -gal responsive Gd-chelate at 37 °C for 8 h. 10 μ l/well of WST-8 solution was added to each well and the plate was incubated at dark, 37 °C for 3 h. The absorbance was measured at 460 nm.

Inductively coupled plasma optical emission spectroscopy (ICP-OES)

The concentration of Gd (III) in the above-mentioned test tubes with control and senescence cells (which had been incubated with 0.5 and 0.25 mM β -gal responsive Gd-chelate) was determined by ICP-OES. Each sample was diluted to 1 mL with concentrated nitric acid and water for ICP-

OES analysis. Gd was measured on a VG Elemental PQExcell spectrometer that was standardized with eight concentrations spanning 0–50 ppb Gd (III). In (III) (1 ppb) was used as an internal standard.

Ex vivo detection of senescent cells in pig knee specimens

Ten knee joints of five Yucatan minipigs (2 male, 3 female) were acquired postmortem from the Veterinary Service Center at Stanford Medicine as a donation in accordance with the 3R principles (Reduce, Refine, Replace). The specimen originated from animals that had undergone other experiments at the facility that did not affect the knee joints. We created two 5 mm full-thickness cartilage defects in the distal femur of each knee specimen. To evaluate the ability of the β -gal responsive Gd-chelate to differentiate senescent and viable cells in arthritic joints, we incubated 1×10^7 control and senescent cells with 0.25 mM β -gal responsive Gd-chelate at 37 °C for 8 h, implanted them into the cartilage defects and scanned the specimen on a 3 T MRI scanner (3 T GE MR 750, GE Healthcare, Boston, MA), using a T_1 -map sequence (TR = 40, 75, 150, 300, 500, 700, and 2000 ms, TE = 10 ms, FOV 80 mm \times 40 mm, matrix 500 \times 250 pixel, 2 averages) and T_1 weighted fast SE sequence (TR = 700 ms, TE = 10 ms, RARE factor = 2, 80 mm \times 40 mm FOV, 500 \times 250 sampling matrix, and 2 averages).

In vivo detection of senescent cells with MRI and the β -gal responsive Gd-chelate

All animal studies were approved by the institution's Administrative Panel on Laboratory Animal Care (APLAC 29859) and were conducted under the supervision of the Stanford Veterinary Service team. Four 4–12-month-old female Yucatan minipigs were obtained from S&S Farms Selma, CA). Following delivery to the facility, all animals underwent a 4-day quarantine and stabilization period. Study animals were housed individually indoors in an AAALAC-accredited facility with a 12/12-h light/dark cycle, controlled temperature (68–76 °F), humidity (30–70%), and ventilation (10–15 air changes hourly). All animals were housed in pens adjacent to pens housing other pigs and were allowed to ambulate at all times. Animals were fed twice daily and had free access to drinking water ad libitum. Environmental enrichment with toys and food rewards was provided on a regular basis. Prior to anesthesia for surgery, imaging, and euthanasia, food was withheld for 12 h.

All animals underwent bilateral knee surgeries to create full-thickness cartilage defects, followed by an MRI on the following day. All procedures were performed under general anesthesia. For surgery, animals were sedated with tiletamine and zolazepam (Telazol; Zoetis, Kalamazoo, MI; 2–8 mg i.m./kg), intubated, and maintained under general anesthesia with 1–3% isoflurane. An eye lubricant was applied to protect the eyes. Animals were monitored continuously, and health status was documented at least every 15 min for heart rate, respiration rate, body temperature, ventilation, oxygenation, and depth of anesthesia by eliciting reflex responses. For each pig, the stifle area was shaved, cleaned with betadine and chlorhexidine, and draped. Sciatic and femoral nerve blocks were performed under ultrasound guidance. Pigs were placed into the supine position on a heating mat and secured to the surgical table. A surgical incision was performed on the medial aspect of the joint, allowing for lateral dislocation of the patella and access to the knee joint.

We created sixteen 5 mm wide full-thickness cartilage defects in eight distal femurs (two defects per knee joint) with a sterile biopsy punch and curette. We implanted 1×10^7 senescent MSCs and 1×10^7 viable MSCs into the cartilage defects and secured them with fibrin glue (Evicel; Ethicon Inc., Somerville, NJ, USA)⁵⁴. In each distal femur, one defect contained senescent MSCs and the other contained viable MSCs. The incision was closed in layers using Vicryl 2-0 and 3-0 (Ethicon Inc.). Upon recovery, animals were allowed unrestricted weight bearing. Animals were monitored for signs of pain and distress and analgesia was provided accordingly.

The next day, animals were anesthetized with isoflurane and underwent intraarticular injection of 2.5 mM of β -gal responsive Gd-chelate intraarticularly into each knee joint. The higher concentration compared to in vitro studies was chosen to account for the dilution of our probe in joint

fluid. At two hours after intraarticular injection of the β -gal responsive Gd-chelate, MRI was performed on a 3 T clinical scanner (3 T GE MR 750, GE Healthcare, Boston, MA) under isoflurane anesthesia, using a knee surface coil and a variable TR saturation recovery sequence (TR = 40, 75, 150, 300, 500, 700, and 2000 ms, TE = 14 ms, FOV 17 cm) and T_1 weighted fast SE sequence (TR = 600 ms, TE = 10.07 ms, FOV 17 cm, slice thickness = 2 mm, spacing = 0.2 and 2 averages). A pilot imaging study was done by performing an MRI of a pig knee joint before the intra-articular injection of the β -gal responsive Gd-chelate.

After completion of MRI, the anesthetized animals were euthanized. A commercially available euthanasia solution (Euthasol, Virbac Corp, Westlake, TX, USA) was administered intravenously under deep anesthesia at 1 mL per 4.5 kg of body weight. Death was confirmed by complete cessation of heartbeat by cardiac auscultation. Following this confirmation, samples of the stifles were excised for postmortem MRI and histopathological assessment. The knee joints were excised and underwent a postmortem scan on a 3 T preclinical MRI scanner (Bruker, BioSpec 3 T MRI, Billerica, MA, USA), using a knee surface coil and with the same MR parameters used to scan the explants, which were described above.

MR image data analyses

MRI scans of contrast agent samples, cell samples, joint specimens, live pigs, and explants were analyzed by generating T_1 -maps with the FIJI software (Bethesda, MD). The T_1 -maps were created by fitting the MRI signal at increasing TRs to the formula $S_n = S_0(1 - \exp(-TR_n/T_1))$ where the S_n : longitudinal magnetization at time n , S_0 : equilibrium longitudinal magnetization, TR: repetition time and T_1 : spin-lattice relaxation time. We then measured the T_1 -relaxation times of contrast agent samples, viable and senescent cells in vitro, ex vivo, and in vivo on the T_1 -maps through operator-defined regions of interest (ROI). We calculated R_1 -relaxation rates as $R_1 = 1/T_1$. We also measured the signal intensity of the cell implants and the background noise on anatomical T_1 -weighted SE images through ROIs and calculated the Signal-to-Noise Ratio (SNR) = $SI_{\text{cell implant}}/\text{noise}$.

Validation of senescence MR imaging biomarker with immunocytochemistry

The excised pig knees were fixed in 10% neutral buffered formalin, followed by decalcification in Formical-2000 for one week. Subsequently, tissues were paraffin-embedded and sectioned into 10- μ m slices using a cryostat microtome (Leica CM1800). For immunocytochemistry (ICC), slides underwent deparaffinization by sequential immersions in xylene (5 min), 100% ethanol (2 min), and 95% ethanol (1 min), followed by rehydration in water. The samples were fixed with 4% paraformaldehyde for 10 min and then washed in triplicate with PBS. Following fixation, tissue sections were permeabilized with 0.25% Triton X-100 in PBS (PBST) for 10 min at room temperature. Subsequently, sections were blocked with 1% BSA in PBST for 30 min at room temperature, then washed and incubated overnight with primary monoclonal antibodies (mAb) p16 mAb (ab51243, Abcam), p21 mAb (ab188224, Abcam), and β -gal mAb (ab203749, Abcam), F4/80 (ab6640, Abcam, Cambridge, UK), CD31 (3528T Cell Signaling), CD73 (13160T Cell Signaling), CD105 (14606S Cell Signaling) and CD90 (13801S Cell Signaling) at 4 °C. After washing, sections were incubated with secondary antibody (Alexa Fluor 488 goat anti-rat IgG, A11006, Invitrogen) for 2 h at room temperature in the dark. Finally, sections were washed and mounted for fluorescence microscopy (Keyence BZ-X710). Histopathologic images of distal femur cartilage were obtained using a defined experimental protocol on the fluorescence microscope (Keyence, Itasca). The mean fluorescence intensity of the green senescent cells was calculated from the sum of the values of all the pixels in the tissue of interest divided by the number of pixels (% of stained/total area) using ImageJ software in a 2 \times field of view²⁵.

Statistical analysis

The Wilcoxon ranksum test was applied to all analyses except the two pig studies, where the clustered Wilcoxon ranksum test was conducted. All

analyses were done using Stata (Stata 18.0, College Station, TX) and R (R 4.3.2, R Core Team (2023)). $p < 0.05$ indicates statistically significant findings.

Data availability

The main data supporting the results of this study are available within the paper and its Supplementary Information. The raw MRI data (DICOM format) are available from the corresponding author on request.

Received: 21 March 2024; Accepted: 18 March 2025;

Published online: 03 May 2025

References

- Ng, N., Parkinson, L., Brown, W. J., Moorin, R. & Peeters, G. M. E. G. Lifestyle behaviour changes associated with osteoarthritis: a prospective cohort study. *Sci. Rep.* **14**, 6242 (2024).
- Jeon, O. H. et al. Local clearance of senescent cells attenuates the development of post-traumatic osteoarthritis and creates a pro-regenerative environment. *Nat. Med.* **23**, 775–781 (2017).
- Gurkar, A. U. et al. Spatial mapping of cellular senescence: emerging challenges and opportunities. *Nat. Aging* **3**, 776–790 (2023).
- SenNet Consortium. NIH SenNet Consortium to map senescent cells throughout the human lifespan to understand physiological health. *Nat. Aging* **2**, 1090–1100 (2022).
- Coryell, P. R., Diekman, B. O. & Loeser, R. F. Mechanisms and therapeutic implications of cellular senescence in osteoarthritis. *Nat. Rev. Rheumatol.* **17**, 47–57 (2021).
- Min, H. K. et al. Dasatinib, a selective tyrosine kinase inhibitor, prevents joint destruction in rheumatoid arthritis animal model. *Int. J. Rheum. Dis.* **26**, 718–726 (2023).
- Matsuno, H. et al. Effects of an oral administration of glucosamine-chondroitin-quercetin glucoside on the synovial fluid properties in patients with osteoarthritis and rheumatoid arthritis. *Biosci. Biotechnol. Biochem.* **73**, 288–292 (2009).
- Yang, H. et al. Navitoclax (ABT263) reduces inflammation and promotes chondrogenic phenotype by clearing senescent osteoarthritic chondrocytes in osteoarthritis. *Aging (Albany, NY)* **12**, 12750–12770 (2020).
- Yan, S. et al. Metformin regulates chondrocyte senescence and proliferation through microRNA-34a/SIRT1 pathway in osteoarthritis. *J. Orthop. Surg. Res.* **18**, 198 (2023).
- Ji, M.-L. et al. Sirt6 attenuates chondrocyte senescence and osteoarthritis progression. *Nat. Commun.* **13**, 7658 (2022).
- Crema, M. D., Roemer, F. W. & Guermazi, A. Magnetic resonance imaging in knee osteoarthritis research: semiquantitative and compositional assessment. *Magn. Reson. Imaging Clin. N. Am.* **19**, 295–321 (2011).
- Perry, T. A. et al. Magnetic resonance imaging-assessed subchondral cysts and incident knee pain and knee osteoarthritis: data from the Multicenter Osteoarthritis Study. *Arthritis Rheumatol.* **74**, 60–69 (2022).
- Lee, B. Y. et al. Senescence-associated beta-galactosidase is lysosomal beta-galactosidase. *Aging Cell* **5**, 187–195 (2006).
- Tang, J.-H. et al. Molecular engineering of self-immolative bioresponsive MR probes. *J. Am. Chem. Soc.* **145**, 10045–10050 (2023).
- Taghian, T. et al. Real-time MR tracking of AAV gene therapy with β gal-responsive MR probe in a murine model of GM1-gangliosidosis. *Mol. Ther. Methods Clin. Dev.* **23**, 128–134 (2021).
- Del Rey, M. J. et al. Senescent synovial fibroblasts accumulate prematurely in rheumatoid arthritis tissues and display an enhanced inflammatory phenotype. *Immun. Ageing* **16**, 29 (2019).
- Li, J. & Pei, M. Cell senescence: a challenge in cartilage engineering and regeneration. *Tissue Eng. Part B Rev.* **18**, 270–287 (2012).

18. Martin, J. A. & Buckwalter, J. A. Telomere erosion and senescence in human articular cartilage chondrocytes. *J. Gerontol. A Biol. Sci. Med. Sci.* **56**, B172–B179 (2001).
19. Brandl, A., Meyer, M., Bechmann, V., Nerlich, M. & Angele, P. Oxidative stress induces senescence in human mesenchymal stem cells. *Exp. Cell Res.* **317**, 1541–1547 (2011).
20. Carlo, M. D. Jr. & Loeser, R. F. Increased oxidative stress with aging reduces chondrocyte survival: correlation with intracellular glutathione levels. *Arthritis Rheum.* **48**, 3419–3430 (2003).
21. Bashiri Dezfouli, A. et al. Doxorubicin-induced senescence through NF- κ B affected by the age of mouse mesenchymal stem cells. *J. Cell. Physiol.* **235**, 2336–2349 (2020).
22. Suryadevara, V. et al. SenNet recommendations for detecting senescent cells in different tissues. *Nat. Rev. Mol. Cell Biol.* <https://doi.org/10.1038/s41580-024-00738-8> (2024).
23. Lupia, M. et al. CD73 regulates stemness and epithelial-mesenchymal transition in ovarian cancer-initiating cells. *Stem Cell Rep.* **10**, 1412–1425 (2018).
24. Meli, V. S. et al. Isolation and characterization of porcine macrophages and their inflammatory and fusion responses in different stiffness environments. *Biomater. Sci.* **9**, 7851–7861 (2021).
25. Roudi, R., Pisani, L., Pisani, F., Kiru, L. & Daldrop-Link, H. E. Novel clinically translatable iron oxide nanoparticle for monitoring anti-CD47 cancer immunotherapy. *Investig. Radiol.* <https://doi.org/10.1097/RLI.0000000000001030> (2023).
26. Muñoz-Espín, D. & Serrano, M. Cellular senescence: from physiology to pathology. *Nat. Rev. Mol. Cell Biol.* **15**, 482–496 (2014).
27. Debacq-Chainiaux, F., Eruslimsky, J. D., Campisi, J. & Toussaint, O. Protocols to detect senescence-associated beta-galactosidase (SA- β gal) activity, a biomarker of senescent cells in culture and in vivo. *Nat. Protoc.* **4**, 1798–1806 (2009).
28. Yang, L. et al. An activatable NIR probe for the detection and elimination of senescent cells. *Anal. Chem.* **94**, 5425–5431 (2022).
29. Redy-Keisar, O., Kisin-Finfer, E., Ferber, S., Satchi-Fainaro, R. & Shabat, D. Synthesis and use of QCy7-derived modular probes for the detection and imaging of biologically relevant analytes. *Nat. Protoc.* **9**, 27–36 (2014).
30. Wehrman, T. S., von Degenfeld, G., Krutzik, P. O., Nolan, G. P. & Blau, H. M. Luminescent imaging of β -galactosidase activity in living subjects using sequential reporter-enzyme luminescence. *Nat. Methods* **3**, 295–301 (2006).
31. Chang, E. Y. et al. SSR white paper: guidelines for utilization and performance of direct MR arthrography. *Skelet. Radiol.* <https://doi.org/10.1007/s00256-023-04420-6> (2023).
32. Zhang, Y., Zhang, B., Liu, F., Luo, J. & Bai, J. In vivo tomographic imaging with fluorescence and MRI using tumor-targeted dual-labeled nanoparticles. *Int. J. Nanomed.* **9**, 33–41 (2014).
33. Dang, X. et al. Deep-tissue optical imaging of near cellular-sized features. *Sci. Rep.* **9**, (2019).
34. Lilley, L. M. et al. Self-immolative activation of β -galactosidase-responsive probes for in vivo MR imaging in mouse models. *Angew. Chem. Int. Ed. Engl.* **59**, 388–394 (2020).
35. Louie, A. Y. et al. In vivo visualization of gene expression using magnetic resonance imaging. *Nat. Biotechnol.* **18**, 321–325 (2000).
36. Ahern, B. J., Parvizi, J., Boston, R. & Schaer, T. P. Preclinical animal models in single site cartilage defect testing: a systematic review. *Osteoarthritis Cartilage* **17**, 705–713 (2009).
37. Baker, D. J. et al. Clearance of p16Ink4a-positive senescent cells delays ageing-associated disorders. *Nature* **479**, 232–236 (2011).
38. Xu, M. et al. Transplanted senescent cells induce an osteoarthritis-like condition in mice. *J. Gerontol. A Biol. Sci. Med. Sci.* **72**, 780–785 (2017).
39. Duan, X. & Luan, S. Efficient secreted expression of natural intracellular β -galactosidase from *Bacillus aryabhattai* via non-classical protein secretion pathway in *Bacillus subtilis*. *Int. J. Biol. Macromol.* **248**, 125758 (2023).
40. Aime, S. & Caravan, P. Biodistribution of gadolinium-based contrast agents, including gadolinium deposition. *J. Magn. Reson. Imaging* **30**, 1259–1267 (2009).
41. Daldrop-Link, H. E. et al. Cell tracking with gadophrin-2: a bifunctional contrast agent for MR imaging, optical imaging, and fluorescence microscopy. *Eur. J. Nucl. Med. Mol. Imaging* **31**, 1312–1321 (2004).
42. Kobayashi, H. et al. Avidin-dendrimer-(1B4M-Gd)(254): a tumor-targeting therapeutic agent for gadolinium neutron capture therapy of intraperitoneal disseminated tumor which can be monitored by MRI. *Bioconjug. Chem.* **12**, 587–593 (2001).
43. Lewin, M. et al. Hepatocyte targeting with Gd-EOB-DTPA: potential application for gene therapy. *Investig. Radiol.* **36**, 9–14 (2001).
44. Kohli, J. et al. Algorithmic assessment of cellular senescence in experimental and clinical specimens. *Nat. Protoc.* **16**, 2471–2498 (2021).
45. Storer, M. et al. Senescence is a developmental mechanism that contributes to embryonic growth and patterning. *Cell* **155**, 1119–1130 (2013).
46. Chen, J.-A. et al. In vivo imaging of senescent vascular cells in atherosclerotic mice using a β -galactosidase-activatable nanoprobe. *Anal. Chem.* **92**, 12613–12621 (2020).
47. Redgrave, R. E. et al. Author Correction: Senescent cardiomyocytes contribute to cardiac dysfunction following myocardial infarction. *NPJ Aging* **9**, 16 (2023).
48. Collado, M. et al. Tumour biology: senescence in premalignant tumours. *Nature* **436**, 642 (2005).
49. Schafer, M. J. et al. Cellular senescence mediates fibrotic pulmonary disease. *Nat. Commun.* **8**, 14532 (2017).
50. Dehkordi, S. K. et al. Profiling senescent cells in human brains reveals neurons with CDKN2D/p19 and tau neuropathology. *Nat. Aging* **1**, 1107–1116 (2021).
51. Novais, E. J. et al. Long-term treatment with senolytic drugs Dasatinib and Quercetin ameliorates age-dependent intervertebral disc degeneration in mice. *Nat. Commun.* **12**, 5213 (2021).
52. Cai, Y. et al. Elimination of senescent cells by β -galactosidase-targeted prodrug attenuates inflammation and restores physical function in aged mice. *Cell Res.* **30**, 574–589 (2020).
53. Rashidi, A. et al. Vascular injury of immature epiphyses impair stem cell engraftment in cartilage defects. *Sci. Rep.* **12**, 11696 (2022).
54. Suryadevara, V. et al. MegaPro, a clinically translatable nanoparticle for in vivo tracking of stem cell implants in pig cartilage defects. *Theranostics* **13**, 2710–2720 (2023).

Acknowledgements

This work was supported by a Technology Development and Application Grant from the National Institutes of Health Senescence Network Funded Research (SENNET) (UG3CA268112). The pig model described here was developed through a grant from the National Institute of Arthritis and Musculoskeletal and Skin Diseases (R01AR054458). The β -gal responsive Gd-chelate was developed through a grant from the National Institute of Neurological Disorders and Stroke (5R01NS115571). We thank Karla Epperson, Kevin Epperson, and Dawn Holley at the Lucas Research Center at Stanford for their assistance with the acquisition of MRI scans for this project. We thank Dr. Frezghi Habte for help acquiring MRI images at the Small Animal Imaging Facility (SAIF) at the Clark Center at Stanford. The Clark Imaging Center is supported by a grant from the Stanford Comprehensive Cancer Center (P30CA124435, PI Steven Artandi). We would like to extend special thanks to Elias Godoy and Kerriann Casey from the Veterinary Service Center (VSC) at Stanford for support in processing the samples for histology specimens. We thank Dr. Emily Alex Waters in the Center for Advanced Molecular Imaging (CAMI) for MR relaxivity data acquisition and analysis at Northwestern University (RRID: SCR_021192). CAMI is generously supported by a grant from the Robert H. Lurie Comprehensive Cancer Center (NCICCSGP30CA060553). Metal analysis was performed by Rebecca Sponenburgper at the Northwestern University Quantitative Bio-

elemental Imaging Center supported by NASA Ames Research Center NNA06CB93G.

Author contributions

K.N., D.B.M., V.S., and H.E.D.L. drafted the main manuscript. K.N., V.S., and H.E.D.L. designed the study. J.H.T. and T.J.M. designed and synthesized the probe. K.N., D.B.M., V.S., M.H., J.W., M.H., T.U., L.P., R.V.K., Z.S.V., I.V., R.R., R.D., S.Y.L.L., and N.S. did the experiments and collected the data. J.K.L., M.M., and I.S. helped perform the live pig experiments. K.N. and V.S. interpreted the data and constructed the figures. T.L. helped with statistics. K.N., V.S., M.M., S.G., G.P., T.J.M., and H.E.D.L. edited the manuscript. All authors reviewed the manuscript.

Competing interests

T.M. Meade, H.E. Daldrup-Link: Provisional Patent NU2024-024-01, S24-019. T.M. Meade: shareholder, PreDx Inc.

Additional information

Supplementary information The online version contains supplementary material available at <https://doi.org/10.1038/s44303-025-00078-y>.

Correspondence and requests for materials should be addressed to Vidyani Suryadevara, Thomas J. Meade or Heike E. Daldrup-Link.

Reprints and permissions information is available at <http://www.nature.com/reprints>

Publisher's note Springer Nature remains neutral with regard to jurisdictional claims in published maps and institutional affiliations.

Open Access This article is licensed under a Creative Commons Attribution-NonCommercial-NoDerivatives 4.0 International License, which permits any non-commercial use, sharing, distribution and reproduction in any medium or format, as long as you give appropriate credit to the original author(s) and the source, provide a link to the Creative Commons licence, and indicate if you modified the licensed material. You do not have permission under this licence to share adapted material derived from this article or parts of it. The images or other third party material in this article are included in the article's Creative Commons licence, unless indicated otherwise in a credit line to the material. If material is not included in the article's Creative Commons licence and your intended use is not permitted by statutory regulation or exceeds the permitted use, you will need to obtain permission directly from the copyright holder. To view a copy of this licence, visit <http://creativecommons.org/licenses/by-nc-nd/4.0/>.

© The Author(s) 2025